

Simulation to scaled city: zero-shot policy transfer for traffic control via autonomous vehicles

Kathy Jang
University of California, Berkeley
kathyjang@berkeley.edu

Logan Beaver
University of Delaware
lebeaver@udel.edu

Behdad Chalaki
University of Delaware
bchalaki@udel.edu

Ben Remer
University of Delaware
bremer@udel.edu

Eugene Vinitsky
University of California, Berkeley
evinitsky@berkeley.edu

Andreas Malikopoulos
University of Delaware
andreas@udel.edu

Alexandre Bayen
University of California, Berkeley
bayen@berkeley.edu

ABSTRACT

Using deep reinforcement learning, we train control policies for autonomous vehicles leading a platoon of vehicles onto a roundabout. Using *Flow*, a library for deep reinforcement learning in micro-simulators, we train two policies, one policy with noise injected into the state and action space and one without any injected noise. In simulation, the autonomous vehicle learns an emergent metering behavior for both policies in which it slows to allow for smoother merging. We then directly transfer this policy without any tuning to the *University of Delaware Scaled Smart City (UDSSC)*, a 1:25 scale testbed for connected and automated vehicles. We characterize the performance of both policies on the scaled city. We show that the noise-free policy winds up crashing and only occasionally metering. However, the noise-injected policy consistently performs the metering behavior and remains collision-free, suggesting that the noise helps with the zero-shot policy transfer. Additionally, the transferred, noise-injected policy leads to a 5% reduction of average travel time and a reduction of 22% in maximum travel time in the UDSSC. Videos of the controllers can be found at <https://sites.google.com/view/iccps-policy-transfer>.

1 INTRODUCTION

Control of mixed-autonomy traffic: Transportation is a major source of US energy consumption and greenhouse gas emissions, accounting for 28% and 26% respectively. According to the bureau of transportation statistics, total road miles traveled is continuously increasing, growing at 2 to 3% per year between 2010 and 2014 while over the same period the total road length of the US transportation network remained unchanged. The increased road usage is coupled with an increase in congestion. Overall congestion delay in 2014 was 6.9 billion hours, an increase of 33% since 2000; the problem is even worse in metropolitan areas where travelers needed to allocate

an additional 150% more travel time during peak periods to arrive on time. The congestion also has significant economic cost, totaling 160 billion dollars in 2014 [5]. Depending on their usage, automated vehicles have the potential to alleviate system level metrics such as *congestion*, *accident rates*, and *greenhouse gas emissions* through a combination of intelligent routing, smoother driving behavior, and faster reaction time[25].

Partially automated systems are predicted to increasingly populate urban streets between 2020 and 2025 but will primarily be usable in restricted situations such as heavy traffic or high speed operations in light traffic. Hazard detection technology is not expected to be mature enough for full automation in the presence of general vehicles and pedestrians (i.e. heterogeneous fleets, manned/unmanned, bicycles, pedestrians, mixed use road-space etc.) until at least 2030. It takes 20 years for a vehicle fleet to turn over sufficiently which makes it likely that vehicles will be partially manned at least until 2050 [19].

Recently, the steady increase in usage of cruise control systems on the roadway offers an opportunity to study the optimization of traffic in the framework of *mixed-autonomy traffic*: traffic that is partially automated but mostly still consists of human driven vehicles. However, the control problems posed in this framework are notoriously difficult to solve. Traffic problems, which often exhibit features such as time-delay, non-linear dynamics, and hybrid behavior, are challenging for classical control approaches, as they rely on models with significant degrees of complexity: discrete events (lane changes, traffic light switches), continuous states (position, speed, acceleration), and non-linear driving models. These complexities make analytical solutions often intractable. The variety and non-linearity of traffic often leads to difficult trade-offs between the complexity of the dynamics model and tractability of the approach.

Classical control approaches: Classical control approaches have successfully solved situations in which the complexity of the problem can be reduced without throwing away key aspects of the dynamics. For example, there is a variety of analytical work on control of autonomous intersections with simple geometries. For mixed-autonomy problems, there have been significant classical controls based results for simple scenarios like vehicles on a ring [4] or a single lane of traffic whose stability can be characterized [13, 22]. A thorough literature review on coordinating

Permission to make digital or hard copies of part or all of this work for personal or classroom use is granted without fee provided that copies are not made or distributed for profit or commercial advantage and that copies bear this notice and the full citation on the first page. Copyrights for third-party components of this work must be honored. For all other uses, contact the owner/author(s).

ICCPs'19, April 2019, Montreal, Canada

© 2018 Copyright held by the owner/author(s).

ACM ISBN 123-4567-24-567/08/06.

https://doi.org/10.475/123_4

automated vehicles in intersections, merging roadways, and roundabouts can be found in [16]. Classical control approaches can be broken down into reservation methods, scheduling, optimization with safety constraints, and safety maximization. Other approaches have involved applications of queuing theory, game theory, and mechanism design.

However, as the complexity of the problem statement increases, classical techniques become increasingly difficult to apply. Shifting focus from simple scenarios to, as an example, hybrid systems with coexisting continuous and discrete controllers, explicit guarantees for hand-designed controllers can become harder to find. Ultimately, when the complexity of the problem becomes too high, optimization-based approaches have been shown to be a successful approach in a wide variety of domains from robotics [9] to control of transportation infrastructure [11].

Deep reinforcement learning: *Deep reinforcement learning* (deep-RL) has recently emerged as an effective technique for control in high dimensional, complex CPS systems. Deep RL has shown promise for control of complex, unstructured problems as varied as robotic skills learning [7], playing games such as Go [20], and traffic light ramp metering [1]. Of particular relevance to this work, deep-RL has been successful in training a single autonomous vehicle to optimize traffic flow in the presence of human drivers [26].

One key distinction in RL is whether the algorithm is model-free or model-based, referring to whether the algorithm is able to query a dynamics model in the computation of the control or the policy update. Model-free RL, which tends to outperform model-based RL if given sufficient optimization time, but requires longer training times. Thus, model-free techniques are most effective when samples can be cheaply and rapidly generated. This often means that model-free RL works best in simulated settings where a simulation step can be made faster than real-time and simulation can be distributed across multiple CPUs or GPUs. A long-standing goal is to be able to train a controller in simulation, where model-free techniques can be used, and then use the trained controller to control the actual system.

Policy Transfer: Transfer of a controller from a training domain to a new domain is referred to as *policy transfer*. The case where the policy is directly transferred without any fine-tuning is referred to as *zero-shot policy transfer*. Zero-shot policy transfer can be quite difficult as the true dynamics of the system may be quite different from the simulated dynamics, known as *model mismatch*. Techniques used to overcome this include adversarial training, in which the policy is trained in the presence of an adversary that can modify the dynamics and the policy must subsequently become robust to perturbations [15]. Other techniques to overcome *model mismatch* include re-learning a portion of the controller [17], adding noise to the dynamics model [14], and learning a model of the true dynamics that can be used to correctly execute the desired trajectory of the simulation-trained controller [3].

Other challenges with policy transfer include *domain mismatch*, where the true environment contains states unobserved in simulation. For example, an autonomous vehicle might see a car color unobserved in its simulations and subsequently react incorrectly. Essentially, the controller over-fits to its observed states and does

not generalize. Techniques used to tackle this problem include domain randomization [23], in which noise is injected into the state space to enforce robustness with respect to unobserved states.

Contributions and organization of the article. In this work we use deep-RL to train an autonomous vehicle to optimize a flow of vehicles entering a roundabout. The RL vehicle interacts with sensors at each of the entrance ramps and is additionally able to acquire state information about vehicles on the roundabout. By incorporating this additional sensor information, we attempt to learn a policy that can optimally time the merges of the RL vehicle. Simultaneously, the RL vehicle must control the behavior of the platoon of human-driven vehicles following the autonomous vehicle (AV). We train the AV with the goal of optimizing the average delay of all the vehicles in simulation.

Next, we attempt to show that this behavior is likely to have real-world relevance by transferring the controllers to the University of Delaware Scaled Smart City (UDSSC), a reduced scale city, whose dynamics, which include sensor delays, friction, and actuation, are likely closer to true vehicle dynamics. We combine the ideas of domain randomization with robustness to an adversary and train a controller in the presence of noise in both its observations and actions. We compare transfer of the policy trained with noise against a policy trained without noise and demonstrate that the noisy policy outperforms both the noise-free policy and an uncontrolled baseline.

In this work we present the following results:

- The use of deep-RL in simulation to learn an emergent metering policy.
- A demonstration that direct policy transfer to UDSSC fails, leading to crashes and poor performance.
- A successful zero-shot policy transfer of the simulated policy to the UDSSC vehicles via injection of noise into both state and action space.
- The analysis of the improvements that the autonomous vehicles bring to the congested roundabout.

The remainder of the article is organized as follows:

- (1) Section 2 provides an introduction to deep-RL and the algorithms on which it operates.
- (2) Section 3 describes the learning of control policies via RL, followed by the policy transfer process from simulation to the physical world.
- (3) Section 4 discusses the results of our experiments.
- (4) Section 5 summarizes our work and future directions.

2 BACKGROUND

2.1 Reinforcement Learning

In this section, we discuss the notation and briefly describe the key concepts used in RL. RL focuses on deriving optimal controllers for *Markov decision processes* (MDP) [2]. The system described in this article solves tasks which conform to the standard structure of a finite-horizon discounted MDP, defined by the tuple $(\mathcal{S}, \mathcal{A}, P, r, \rho_0, \gamma, T)$. Here \mathcal{S} is a set of states and \mathcal{A} is a set of actions where both sets can be finite or infinite. $P : \mathcal{S} \times \mathcal{A} \times \mathcal{S} \rightarrow \mathbb{R}_{\geq 0}$ is the transition probability distribution describing the probability of moving from one state s to another state s' given action a , $r : \mathcal{S} \times \mathcal{A} \rightarrow \mathbb{R}$ is the

reward function, $\rho_0 : \mathcal{S} \rightarrow \mathbb{R}_{\geq 0}$ is the probability distribution over start states, $\gamma \in (0, 1]$ is the discount factor, and T is the horizon. For partially observable tasks, which conform to the structure of a *partially observable Markov decision process* (POMDP), two more components are required, namely Ω , a set of observations of the hidden states, and $O : \mathcal{S} \times \Omega \rightarrow \mathbb{R}_{\geq 0}$, the observation probability distribution.

RL studies the problem of how an agent can learn to take actions in its environment to maximize its expected cumulative discounted reward: specifically it tries to optimize $R = \mathbb{E} \left[\sum_{t=0}^T \gamma^t r_t \right]$ where r_t is the reward at time t . The goal is to use the observed data from the MDP to optimize a *policy* $\Pi : \mathcal{S} \rightarrow \mathcal{A}$, mapping states to actions, that maximizes R . This policy can be viewed as the controller for the system, however, we stick to the convention of RL literature and refer to it as a policy. It is increasingly common to parameterize the policy via a neural net. We will denote the parameters of this policy, which are the weights of the neural network, by θ and the policy by π_θ . A neural net consists of a stacked set of affine linear transforms and non-linearities that the input is alternately passed through. The presence of multiple stacked layers is the origin of the term "deep"-RL.

2.2 Policy Gradient Methods

Policy gradient methods use Monte Carlo estimation to compute an estimate of the gradient of the expected discounted reward $\nabla_\theta R = \nabla_\theta \mathbb{E} \left[\sum_{t=0}^T \gamma^t r_t \right]$ where θ are the parameters of the policy π_θ . We perform repeated *rollouts*, in which the policy is used to generate the actions at each time step. At the end of the rollout, we have accumulated a state, action, reward trajectory $\tau = (s_0, a_0, r_0, \dots, s_T)$. Policy gradient methods take in a set of these trajectories and use them to compute an estimate of the gradient $\nabla_\theta R$ which can be used in any gradient ascent-type method.

The particular policy gradient method used in this paper is *Trust Region Policy Optimization* (TRPO) [18]. TRPO is a monotonic policy improvement algorithm, whose update step provides guarantees of an increase in the expected total reward. However, the exact expression for the policy update leads to excessively small steps so implementations of TRPO take larger steps by using a trust region. In this case, the trust region is a bound on the KL divergence between the old policy and the policy update. While not a true distance measure, a small KL divergence between the two policies suggests that the policies do not act too differently over the observed set of states, preventing the policy update step from sharply shifting the policy behavior.

2.3 Car Following Models

For our model of the driving dynamics, we used the *Intelligent Driver Model* [24] (IDM) that is built into the traffic microsimulator SUMO [8]. IDM is a microscopic car-following model commonly used to model realistic driver behavior. Using this model, the acceleration for vehicle α is determined by its bumper-to-bumper *headway* s_α (distance to preceding vehicle), the vehicle's own velocity v_α , and relative velocity Δv_α , via the following equation:

$$a_{\text{IDM}} = \frac{dv_\alpha}{dt} = a \left[1 - \left(\frac{v_\alpha}{v_0} \right)^\delta - \left(\frac{s^*(v_\alpha, \Delta v_\alpha)}{s_\alpha} \right)^2 \right] \quad (1)$$

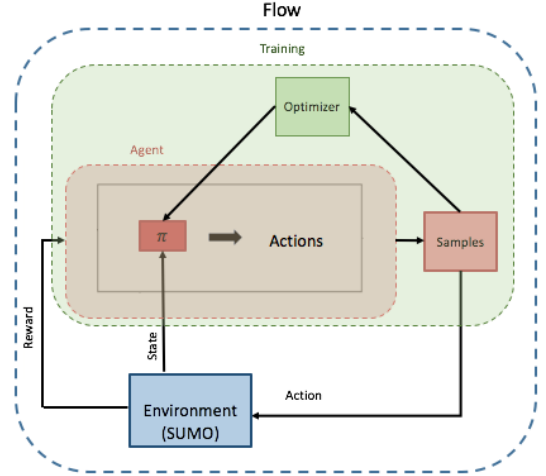


Figure 1: Diagram of the iterative process in *Flow*. Portions in red correspond to the controller and rollout process, green to the training process, and blue to traffic simulation.

where s^* is the desired headway of the vehicle, denoted by:

$$s^*(v_\alpha, \Delta v_\alpha) = s_0 + \max \left(0, v_\alpha T + \frac{v_\alpha \Delta v_\alpha}{2\sqrt{ab}} \right) \quad (2)$$

where $s_0, v_0, T, \delta, a, b$ are given parameters. Typical values for these parameters can be found in [24]; the values used in our simulations are given in Sec. 3.1.1. To better model the natural variability in driving behavior, we induce stochasticity in the desired driving speed v_0 . On any edge, the value of v_0 for a given vehicle is sampled from a Gaussian whose mean is the speed limit of the lane and whose standard deviation is 20% of the speed limit.

C following models are not inherently collision-free, we supplement them with a safe following rule: a vehicle is not allowed to take on velocity values that might lead to a crash if its lead vehicle starts braking at maximum deceleration. However, due to some uncertainty in merging behavior, there are still rare crashes that can occur in the system.

2.4 Flow

We run our experiments in *Flow* [26], a library that provides an interface between a traffic microsimulator, SUMO [8], and popular RL libraries, rllab [6] and RLlib [12], which are centralized and distributed RL libraries respectively. *Flow* enables users to create new traffic networks via a python interface, introduce autonomous controllers into the networks, and then train the controllers in a distributed fashion on the cloud via AWS EC2. To make it easier to reproduce our experiments or try to improve on our benchmarks, the code for *Flow*, scripts for running our experiments, and tutorials can be found at <https://github.com/flow-project/flow>.

Fig. 1 describes the process of training the policy in *Flow*. The controller, here represented by policy π_θ , receives a state and reward from the environment and uses the state to compute an action. The action is taken in by the traffic micro-simulator, which outputs the next state and a reward. The (state, next state, action, reward)

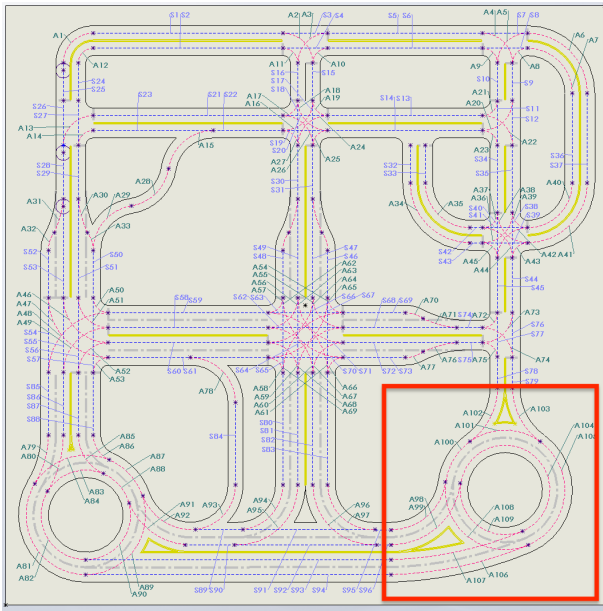


Figure 2: Diagram of the UDSSC road map, with the experimental zone highlighted in red.

tuple are stored as a sample to be used in the optimization step. After accumulating enough samples, the states, actions, and rewards are passed to the optimizer to compute a new policy.

2.5 University of Delaware’s Scaled Smart City (UDSSC)

The *University of Delaware’s Scaled Smart City (UDSSC)* was used to validate the performance of the RL control system. UDSSC is a testbed (1:25 scale) that can help prove concepts beyond the simulation level and can replicate real-world traffic scenarios in a small and controlled environment. UDSSC uses a VICON camera system to track the position of each vehicle with sub-millimeter accuracy, which is used both for control and data collection. The controller for each vehicle is offloaded to a mainframe computer and runs on an independent thread which is continuously fed data from the VICON system. Each controller uses the global VICON data to generate a speed reference for the vehicles allowing for precise independent closed-loop feedback control. A detailed description of UDSSC can be found in [21]. To validate the effectiveness of the proposed RL approach in a physical environment, the southeast roundabout of the UDSSC was used (Fig. 2).

3 EXPERIMENTAL DEPLOYMENT

3.1 Experimental setup

3.1.1 Simulation Details. To derive the RL policy, we developed a model of the roundabout highlighted in red in Fig. 2 in SUMO. The training of the model, shown in Fig. 3, included a single-lane roundabout with entry points at the northern and western ends. Throughout this paper we will refer to vehicles entering from the western end as the *western platoon* and the north entrance as the

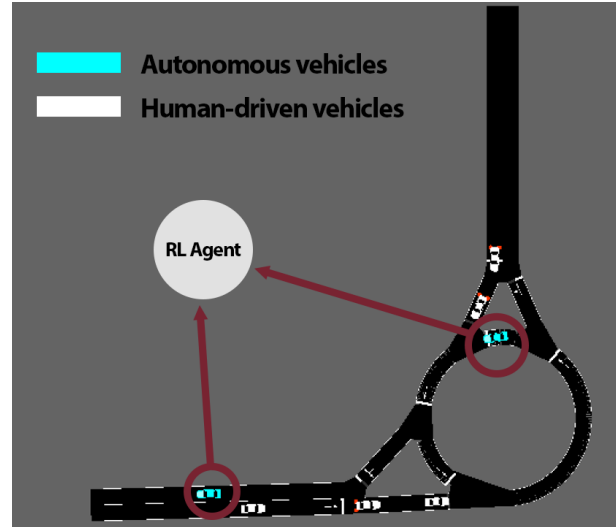


Figure 3: SUMO-generated network in UDSSC’s roundabout. The blue vehicles are the AVs; they are both controlled by the RL policy. Videos of this policy in simulation are available at <https://sites.google.com/view/iccps-policy-transfer>.

northern platoon. The entry points of the model are angled slightly different as it can be seen in Figs. 2 and 3.

The human-controlled vehicles operate in SUMO’s built-in IDM controller, with several modified parameters. In these experiments, the vehicles operating with the IDM controller are run with $T = 1$, $a = 1$, $b = 1.5$, $\delta = 4$, $s_0 = 2$, and $v_0 = 30$, where T is a safe time headway, a is a comfortable acceleration in m/s^2 , b is a comfortable deceleration, δ is an acceleration exponent, s_0 is the linear jam distance, and v_0 is a desired driving velocity. Details of the physical interpretation of these parameters can be found in [24]. The *noise* parameter denotes the standard deviation of normal perturbations to the acceleration. Environment parameters in simulation were set to match the physical constraints of UDSSC. These include: a maximum acceleration of $1 \frac{m}{s^2}$, a maximum deceleration of $-1 \frac{m}{s^2}$, and a maximum velocity of $15 \frac{m}{s}$. The time-step of the system is set 1.0 seconds.

Simulations on this scenario in the roundabout were executed across a range of different settings in terms of volume and stochasticity of inflows. In the RL policy implemented in UDSSC and discussed in 3.1.2, vehicles are introduced to the system via deterministic inflows from the northern and western ends of the roundabout using two routes: (1) vehicles entering the system from the northern inflow merge into the roundabout and exit through the western outflow and (2) vehicles entering the system from the western inflow U-turn through the roundabout and exit through the western outflow. On the western inflow, three vehicles running with the IDM controller led by a vehicle running with the RL policy that entered every 1.2 minutes. On the northern inflow, two vehicles running with the IDM controller led by a vehicle running with the RL policy that entered every 1.2 minutes. These inflow settings are designed to showcase the scenario where routes clash (Fig. 3).

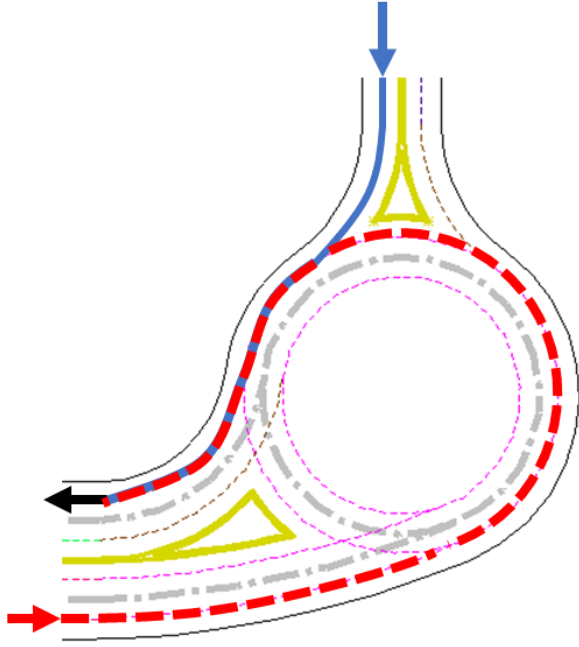


Figure 4: Visualization of the path taken on the UDSSC roundabout. The red route enters going east and exits going west; the blue route enters north and exits via the same west entrance as the red route.

3.1.2 UDSSC. Each vehicle in UDSSC uses a saturated IDM controller to (1) avoid negative speeds, (2) ensure that the rear-end collision constraints do not become active, and (3) maintain the behavior of Eq. (1). Both the IDM and RL controllers provide a desired acceleration for the vehicles, which is numerically integrated to calculate each vehicle’s reference speed.

Merging at the northern entrance of the roundabout is achieved by an appropriate yielding function. Using this function, the car entering the roundabout proceeds only if no other vehicle is on the roundabout in a distance that a potential lateral collision may occur. Otherwise, the vehicle stops at the entry of the roundabout waiting to find a safe space to proceed.

To match the SUMO training environment, only one vehicle per path was allowed to use the RL policy. The paths taken by each vehicle are shown in Fig. 4. For each path the first vehicle to enter the experimental zone was controlled by the RL policy; every subsequent vehicle running with the RL policy runs with the saturated IDM controller. Once an active vehicle running with the RL policy exits the experimental zone it reverts back to the IDM controller and the next vehicle running with the RL policy which is located furthest along the route becomes active.

In the experiments, the vehicles operated in a predefined deterministic order ,i.e., four vehicles were placed just outside the experimental zone on the western loop and three vehicles were placed in the same fashion near the northern entrance. Each vehicle platoon was led by a vehicle running with the RL policy, except in the baseline case where all vehicles used the saturated IDM controller. The experiment was executed with three variations: (1) the

baseline case with only vehicles running with the IDM controller, (2) the case with a leader vehicle running with the RL policy trained in sumo, and (3) the case where the leader vehicles running with the RL policy were trained with noise actively injected into their observations and accelerations.

3.2 Reinforcement Learning Structure

3.2.1 Action space. We parametrize the controller as a neural net mapping the observations to a mean and diagonal covariance matrix of a Gaussian. The actions are sampled from the Gaussian; this is a standard controller parametrization [10]. The actions are a two-dimensional vector of accelerations in which the first element corresponds to vehicles on the north route and the second element to vehicles on the west route. Because the dimension of the action vector is fixed there can only ever be 1 AV from the northern entry, and 1 AV from the western entry. Two queues, one for either entryway, maintain a list of the RL-capable that are currently in the system. Control is given to vehicles at the first position in either queue. When a vehicle completes its route and exits the experimental zone, its id is popped from the queue. All other RL-capable vehicles are passed IDM actions until they reach the front of the queue. If there are fewer than two AVs in the system, the extra actions are simply unused.

The dynamics model of the autonomous vehicles are given by the IDM described in sec. 2.3 subject to a minimum and maximum speed i.e.

$$v_j^{\text{IDM}}(t + \Delta t) = \max \left(\min \left(v_{AV}(t) + a_{\text{IDM}} \Delta t, v_j^{\text{max}}(t) \right), 0 \right) \quad (3)$$

where $v_j^{\text{AV}}(t)$ is the velocity of autonomous vehicle j at time t , a_{IDM} is the acceleration given by an IDM controller, Δt is the time-step, and $v_j^{\text{max}}(t)$ is the maximum speed set by the city j . For the AVs, the acceleration a_t is straightforwardly added to the velocity via a first-order Euler integration step

$$v_j^{\text{AV}}(t + \Delta t) = \max \left(\min \left(v_j^{\text{AV}}(t) + a_t \Delta t, v_j^{\text{max}}(t) \right), 0 \right) \quad (4)$$

3.2.2 Observation space. For the purposes of keeping in mind physical sensing constraints, the state space of the MDP is partially observable and includes the following:

- The positions of the AVs.
- The velocities of the AVs.
- The distances from the roundabout of the 6 closest vehicles to the roundabout for both roundabout entryways.
- The velocities of the 6 closest vehicles to the roundabout for both roundabout entryways.
- Tailway and headway (i.e. distances to the leading and following vehicles) of vehicles from both AVs.
- Length of the number of vehicles waiting to enter the roundabout for both roundabout entryways.
- The distances and velocities of all vehicles in the roundabout.

This state space was designed with real-world implementation in mind, and could conceivably be implemented on existing roadways equipped with loop detectors, sensing tubes, and vehicle-to-vehicle communication between the AVs. For a sufficiently small roundabout, it is possible that an AV equipped with enough cameras could

identify the relevant positions and velocities of roundabout vehicles. Similarly, the queue lengths can be accomplished with loop detectors, and the local information of the AVs (its own position and velocity, as well as the position and velocity of its leader and follower) are already necessarily implemented in distance-keeping cruise control systems.

3.2.3 Action and State Noise. We train the policies in two scenarios, a scenario where both the action and state space are perturbed with noise and a scenario with no noise. This former setting corresponds to a type of *domain randomization*. In the noise case we draw both action and state space noise from a Gaussian with mean zero and standard deviation 0.1.

3.2.4 Reward function. For our reward function we use a combination of the L2-norm of the velocity of all vehicles in the system and penalties discouraging standstills or low velocity travel.

$$r_t = \frac{\max\left(v_{\max}\sqrt{n} - \sqrt{\sum_{i=1}^n (v_{i,t} - v_{\max})^2}, 0\right)}{v_{\max}\sqrt{n}} - 1.5 \cdot \text{pen}_s - \text{pen}_p \quad (5)$$

where n is the number of all vehicles in the system, v_{\max} is the maximum velocity of $15 \frac{\text{m}}{\text{s}}$, $v_{i,t}$ is the velocity that vehicle v_i is travelling at at time t . The first term incentivizes vehicles to travel near speed v_{\max} but also encourages the system to prefer a mixture of low and high velocities versus a mixture of mostly equal velocities. The preference for low and high velocities is intended to induce a platooning behavior. RL algorithms are sensitive to the scale of the reward functions; to control this reward is normalized by $v_{\max}\sqrt{n}$ so that the maximum reward of a time-step is 1.

This reward function also introduces 2 penalty functions, pen_s and pen_p . pen_s returns the number of vehicles that are traveling at a velocity of 0, and pen_p is the number of vehicles that are traveling below a velocity of 0.3. They are defined as:

$$\text{pen}_s = \sum_{i=1}^n g(i) \quad \text{where} \quad g(x) = \begin{cases} 0, & v_x \neq 0, \\ 1, & v_x = 0. \end{cases} \quad (6)$$

$$\text{pen}_p = \sum_{i=1}^n h(i) \quad \text{where} \quad h(x) = \begin{cases} 0, & v_x \geq 0.3, \\ 1, & v_x \leq 0.3 \end{cases} \quad (7)$$

These penalty functions are added to discourage the autonomous vehicle from fully stopping or adopting too-low speeds.

3.3 Algorithm/simulation details

We ran the RL experiments with a discount factor of .999, a trust-region size of .01, a batch size of 20000, a horizon of 500 seconds, and trained over 100 iterations. The controller is a neural network, a *Gaussian multi-layer perceptron* (MLP), with hidden sizes of (100, 50, 25) and a tanh non-linearity. The states are normalized so that they are between 0 and 1 via constant normalization factors. The actions are clipped to be between -1 and 1 . Both normalization and clipping occur after the noise is added to the system so that the bounds are properly respected.

3.4 Code reproducibility

In line with open, reproducible science, the following codebases are needed to reproduce the results of our work. *Flow* can be found

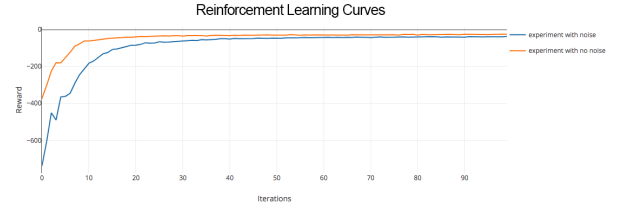


Figure 5: Convergence of the RL reward curve of an experiment with noised IDM, RL accelerations, and noisy state space

at <https://github.com/flow-project/flow>. The version of *rllab* used for the RL algorithms is available at <https://github.com/cathywu/rllab-multiagent> at commit number **4b5758f**. *SUMO* can be found at <https://github.com/eclipse/sumo> at commit number **1d4338ab80**.

3.5 Policy Transfer

The RL policy derived in the SUMO was encoded as the weights of a neural network. The weights were extracted into an appropriate file embedded into a python function with identical inputs and outputs that were used in the training. The python function was used as a control module within the UDSSC replacing the IDM control module in vehicles operating under the RL policy.

In the experiments, each vehicle that was selected to use the RL policy was added to a queue – one queue for each entrance – and remained there until exiting the experimental zone and reverting back to the IDM controller. The first vehicle of each queue is the active vehicle running with the RL policy while the remaining vehicles used the IDM controller. The active vehicles running with the RL policy received the following information: (1) position and speed of the other vehicles in the experimental zone and (2) the number of vehicles in each queue at the entry points of the roundabout.

The inputs to the RL neural network were captured by the VICON system and mainframe. The global 2D positions of each vehicle were captured at each time step. These positions were numerically derived to get each vehicle’s speed and were compared to the physical bounds on the roadways to get the number of vehicles in each queue at the entry points. Finally, the 2D positions were mapped into the 1D absolute coordinate frame used during training. This array was passed into the RL control module as the inputs of the neural network.

3.6 Results

In this section we present our results on a) training vehicular control policies via RL b) transferring the successful policy to UDSSC. Extended work and videos of the policies in action are available at <https://sites.google.com/view/iccps-policy-transfer>.

3.6.1 Simulation results. Fig. 5 depicts the reward curve. The noise-injected RL policy takes longer to train than the noise-free policy but converges to an almost-identical final reward. In the simulations, videos of which are on the website, a behavior emerges in which the incoming western vehicle learns to slow down to allow the vehicles on the north ramp to smoothly merge.

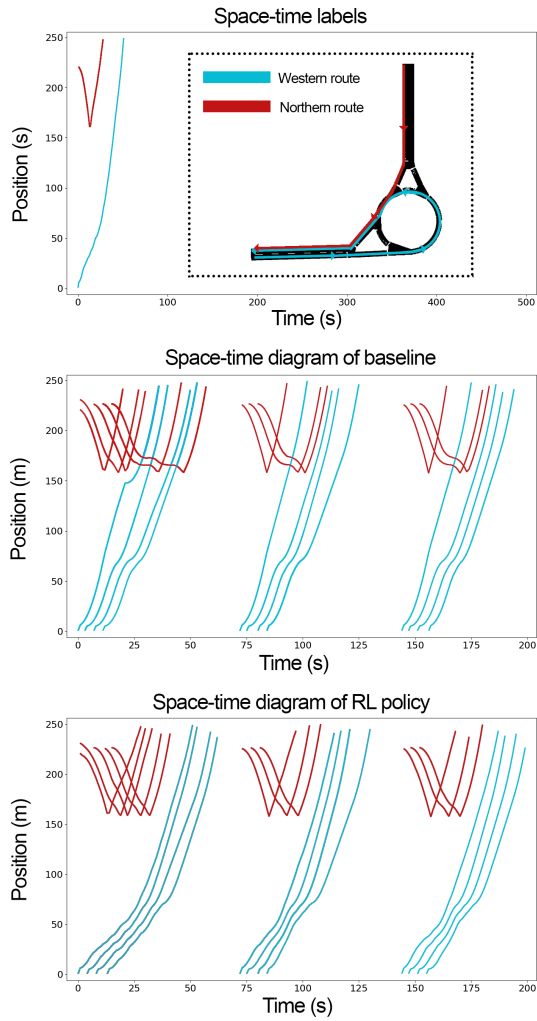


Figure 6: Space-time diagrams of the simulated baseline and RL policy. Top: a guide to the color-scheme of the space time diagrams. The northern route is in red, the western route in blue. Middle: illustrates the overlap between the merging northern platoon and the western platoon. Bottom: The RL policy, depicted at the bottom successfully removes this overlap. Videos of this policy in simulation are available at <https://sites.google.com/view/iccps-policy-transfer>.

This behavior can also be seen in the space-time diagrams in Fig. 6 where western vehicles are in blue and northern in red. Due to the overlapping routes, visible in Fig. 4, it was necessary to put a kink in the diagram where the two routes overlap crosses back; the kink is at the point where the northern and western routes meet. As can be seen in the middle figure, in the baseline case the two routes conflict as the northern vehicles aggressively merge onto the ramp and cut off the western platoon. Once the RL policy controls the autonomous vehicles, it slows down the western platoon so that no overlap occurs and the merge conflict is removed.

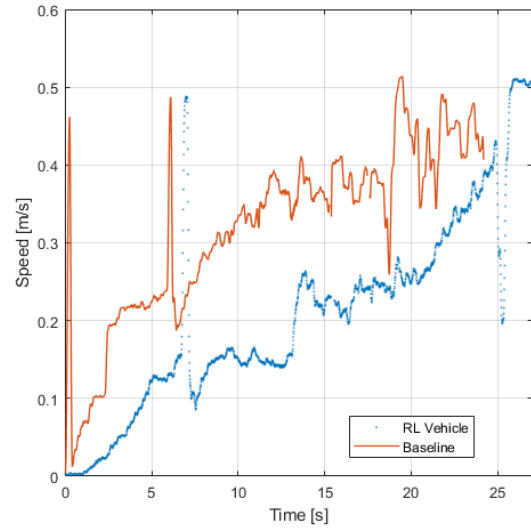


Figure 7: Comparison of the first vehicle on the southern loop for the baseline (IDM) and RL experiments. The RL vehicle starts off slower but eventually accelerates sharply once the northern platoon has passed.



Figure 8: Experiment with two platoons being led by RL vehicles (blue, circled).

3.6.2 Transfer to UDSSC. The RL policies were tested under three cases in UDSSC: (1) the baseline case with only vehicles running with the IDM controller, (2) the case with a leader vehicle running with the RL policy trained in sumo without additional noise, and (3) the case where the leader vehicles running with the RL policy were trained with noise actively injected into their observations and accelerations. The averaged results of these trials are presented in Table 1.

During the congestion experiment, the platoons led by RL vehicles trained with injected noise significantly outperformed the baseline trained and noise-free cases. The results of these experiments,

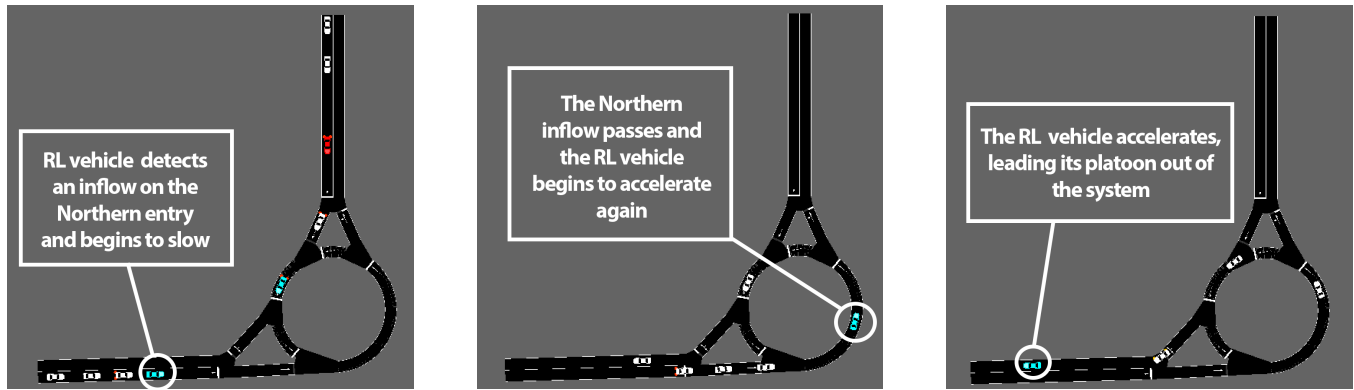


Figure 9: RL-controlled vehicle demonstrating smoothing behavior in this series of images. First: RL vehicle slows down in anticipation of a sufficiently short inflow from the north. Second: The northern inflow passes through the roundabout at high velocity. Fourth: The RL vehicle accelerates and leads its platoon away from the roundabout. Videos of this policy in simulation are available at <https://sites.google.com/view/iccps-policy-transfer>.

	Avg. Vel.[m/s]	Avg. Time[s]	Max Time[s]
Baseline	0.26	15.71	23.99
RL	0.22	15.68	20.62
RL with Noise	0.23	14.81	18.68

Table 1: Results for the congestion experiment, the average and maximum times are averaged between three RL trials and a single baseline trial.

averaged over three trials with the RL vehicles, are presented in Table 1. This improvement was the outcome of a metering behavior learned by the western RL platoon leader. In the baseline case, the north and western platoons meet and lead to a merge conflict that slows the incoming western vehicles down. This sudden decrease in speed can be seen in the drop in velocity at 20 seconds of the baseline in Fig. 7.

In the RL controlled case, the western platoon adopted a lower speed than the baseline IDM controller, as can be seen in the lower velocity of the RL vehicle in Fig. 7. This allowed the northern queue to merge before the western platoon arrived, increasing the overall throughput of the roundabout. This is closer to a socially optimal behavior, leading to a lower average travel time than the greedy behavior shown in the baseline scenario.

Fig. 8 shows the experiment in progress, with the blue (circled) vehicles being RL vehicles trained under noisy conditions. The RL vehicle entering from the western (lower) entrance has performed its metering behavior, allowing vehicles from the northern (upper) queue to pass into the roundabout before the western RL vehicle speeds up again. Videos of the emergent behavior can be found on the website.

4 DISCUSSION

For the simulated experiment, the choice of reward function encourages sharp variation in the system velocities, as the 2-norm is willing to accept a few small velocities if some of the vehicles

can acquire much larger velocities. As a result, a metering behavior emerges where the western platoon initially travels slowly to enable the western platoon to travel quickly. Table 1 reports the results of the UDSSC experiments on three metrics

- The average velocity of the vehicles in the system
- The average time spent in the system
- The maximum time that any vehicle spent in the system

Note, the system is defined as entire area of the experiments, including the entrances to the roundabouts. While the RL and noised-RL under-performed in average velocity, the noised-RL outperformed the baseline on the most relevant metric: average travel time. Thus, the noised policy was able to successfully transfer from simulation to UDSSC (add discussion of how much, by comparing to the simulation) and improved the average travel time by 5% and the max travel time by 22%. The noise-free policy did not improve on the average travel time and only improved the maximum travel time by 14%. Although we did not perform an ablation test to check whether both state space noise and action space noise were necessary, this does confirm that the randomization improved the policy transfer process.

The UDSSC reproduced the metering behavior for the noise-injected policy, but did not do so for the policy that was trained without noise. As can be seen in the videos, the noise-free policy was not robust and would only irregularly reproduce the merging behavior. In addition, the noise-free policy would occasionally crash.

However, we caution that in our testing of the policy transfer process we performed a relatively limited test of the effectiveness of the policy. The vehicles were all lined up outside the system and then let loose; thus, the tests were mostly deterministic; any randomness in the tests would solely be due to randomness in the dynamics of the UDSSC cars. The trained policy was not directly given this inflow distribution at train time, so this does correspond to a separation between train and test sets. However, it is possible that some other initial distribution of vehicles in the UDSSC would have led to worse performance of the RL policy.

5 CONCLUSIONS

In this work we showcased that AVs trained with deep-RL can optimize merging on a roundabout by platooning the merging vehicles to ensure a smooth merge. We trained two policies, one in the presence of state and action space noise, and one without, and demonstrated that the addition of noise led to a successful transfer of the emergent metering behavior while the noise-free policy often collided or failed to meter. This suggests that for non-vision based robotic systems with small action-dimension, small amounts of noise in state and action space may be sufficient for effective zero-shot policy transfer. As a side benefit, we also demonstrate that the emergent behavior leads to a reduction of 5% in average travel time and 22% max-travel time on the transferred network.

In future work, we aim to characterize this result more extensively, testing the policy against a wide range of vehicle spacings and inflow rates. Furthermore, there are several questions we will aim to answer with regards to the policy transfer process. Namely:

- Are both state and action space noise needed for effective policy transfer?
- What scale and type of noise is most helpful in making the policy transfer?
- Would adversarial noise lead to a more robust policy?
- Can we theoretically characterize the types of noise that lead to zero-shot policy transfer?

Finally, we will aim to generalize this result to more complex roundabouts including many lanes, many entrances, and the ability of vehicles to lane-change.

ACKNOWLEDGMENTS

This research was funded in part by an NSF Graduate Research Fellowship. AWS credits and funding were provided by an Amazon Machine Learning Research award.

The authors would also like to thank the Ray Zayas and Ishtiaque Mahbub for their contributions to the UDSSC codebase.

REFERENCES

- [1] Francois Belletti, Daniel Haziza, Gabriel Gomes, and Alexandre M Bayen. 2017. Expert level control of ramp metering based on multi-task deep reinforcement learning. *IEEE Transactions on Intelligent Transportation Systems* (2017).
- [2] Richard Bellman. 1957. A Markovian decision process. *Journal of Mathematics and Mechanics* (1957), 679–684.
- [3] Paul Christiano, Zain Shah, Igor Mordatch, Jonas Schneider, Trevor Blackwell, Joshua Tobin, Pieter Abbeel, and Wojciech Zaremba. 2016. Transfer from simulation to real world through learning deep inverse dynamics model. *arXiv preprint arXiv:1610.03518* (2016).
- [4] Shumo Cui, Benjamin Seibold, Raphael Stern, and Daniel B Work. 2017. Stabilizing traffic flow via a single autonomous vehicle: Possibilities and limitations. In *Intelligent Vehicles Symposium (IV), 2017 IEEE*. IEEE, 1336–1341.
- [5] US DOT. 2016. National transportation statistics. *Bureau of Transportation Statistics, Washington, DC* (2016).
- [6] Yan Duan, Xi Chen, Rein Houthoofd, John Schulman, and Pieter Abbeel. 2016. Benchmarking deep reinforcement learning for continuous control. In *International Conference on Machine Learning*. 1329–1338.
- [7] Shixiang Gu, Ethan Holly, Timothy Lillicrap, and Sergey Levine. 2017. Deep reinforcement learning for robotic manipulation with asynchronous off-policy updates. In *Robotics and Automation (ICRA), 2017 IEEE International Conference on*. IEEE, 3389–3396.
- [8] Daniel Krajzewicz, Jakob Erdmann, Michael Behrisch, and Laura Bieker. 2012. Recent Development and Applications of SUMO - Simulation of Urban MObility. *International Journal On Advances in Systems and Measurements* 5, 3&4 (December 2012), 128–138.
- [9] Scott Kuindersma, Robin Deits, Maurice Fallon, Andrés Valenzuela, Hongkai Dai, Frank Permenter, Twan Koolen, Pat Marion, and Russ Tedrake. 2016. Optimization-based locomotion planning, estimation, and control design for the atlas humanoid robot. *Autonomous Robots* 40, 3 (2016), 429–455.
- [10] Sergey Levine and Pieter Abbeel. 2014. Learning neural network policies with guided policy search under unknown dynamics. In *Advances in Neural Information Processing Systems*. 1071–1079.
- [11] Li Li, Yisheng Lv, and Fei-Yue Wang. 2016. Traffic signal timing via deep reinforcement learning. *IEEE/CAA Journal of Automatica Sinica* 3, 3 (2016), 247–254.
- [12] Eric Liang, Richard Liaw, Robert Nishihara, Philipp Moritz, Roy Fox, Joseph Gonzalez, Ken Goldberg, and Ion Stoica. 2017. Ray RLlib: A Composable and Scalable Reinforcement Learning Library. *arXiv preprint arXiv:1712.09381* (2017).
- [13] Gábor Orosz. 2016. Connected cruise control: modelling, delay effects, and nonlinear behaviour. *Vehicle System Dynamics* 54, 8 (2016), 1147–1176.
- [14] Xue Bin Peng, Marcin Andrychowicz, Wojciech Zaremba, and Pieter Abbeel. 2017. Sim-to-real transfer of robotic control with dynamics randomization. *arXiv preprint arXiv:1710.06537* (2017).
- [15] Lrelle Pinto, James Davidson, Rahul Sukthankar, and Abhinav Gupta. 2017. Robust adversarial reinforcement learning. *arXiv preprint arXiv:1703.02702* (2017).
- [16] Jackeline Rios-Torres and Andreas A. Malikopoulos. 2017. A Survey on the Coordination of Connected and Automated Vehicles at Intersections and Merging at Highway On-Ramps. *IEEE Transactions on Intelligent Transportation Systems* (2017), 1066–1077.
- [17] Andrei A Rusu, Matej Vecerik, Thomas Rothörl, Nicolas Heess, Razvan Pascanu, and Raia Hadsell. 2016. Sim-to-real robot learning from pixels with progressive nets. *arXiv preprint arXiv:1610.04286* (2016).
- [18] John Schulman, Sergey Levine, Pieter Abbeel, Michael Jordan, and Philipp Moritz. 2015. Trust region policy optimization. In *International Conference on Machine Learning*. 1889–1897.
- [19] Steven E Shladover. 2017. Connected and Automated Vehicle Systems: Introduction and Overview. *Journal of Intelligent Transportation Systems* just-accepted (2017), 00–00.
- [20] David Silver, Julian Schrittwieser, Karen Simonyan, Ioannis Antonoglou, Aja Huang, Arthur Guez, Thomas Hubert, Lucas Baker, Matthew Lai, Adrian Bolton, et al. 2017. Mastering the game of Go without human knowledge. *Nature* 550, 7676 (2017), 354.
- [21] Adam Stager, Luke Bhan, Andreas Malikopoulos, and Lihui Zhao. 2018. A Scaled Smart City for Experimental Validation of Connected and Automated Vehicles. 51, 9 (2018), 130 – 135. 15th IFAC Symposium on Control in Transportation Systems CTS 2018.
- [22] D Swaroop and J Karl Hedrick. 1996. String stability of interconnected systems. *IEEE transactions on automatic control* 41, 3 (1996), 349–357.
- [23] Josh Tobin, Rachel Fong, Alex Ray, Jonas Schneider, Wojciech Zaremba, and Pieter Abbeel. 2017. Domain randomization for transferring deep neural networks from simulation to the real world. In *Intelligent Robots and Systems (IROS), 2017 IEEE/RSJ International Conference on*. IEEE, 23–30.
- [24] Martin Treiber, Ansgar Hennecke, and Dirk Helbing. 2000. Congested traffic states in empirical observations and microscopic simulations. *Physical review E* 62, 2 (2000), 1805.
- [25] Zia Wadud, Don MacKenzie, and Paul Leiby. 2016. Help or hindrance? The travel, energy and carbon impacts of highly automated vehicles. *Transportation Research Part A: Policy and Practice* 86 (2016), 1–18.
- [26] Cathy Wu, Aboudy Kreidieh, Kanaad Parvate, Eugene Vinitzky, and Alexandre M Bayen. 2017. Flow: Architecture and Benchmarking for Reinforcement Learning in Traffic Control. *arXiv preprint arXiv:1710.05465* (2017).